Uncovering the Interplay Between Epigenome Editing Efficiency and Sequence Context Using a Novel Inducible Targeting System

Bin Yang[1], Alicia Borgeaud[1,2], Lorène Aeschbach[1], and Vincent Dion[1]*

1: University of Lausanne, Faculty of Biology and Medicine, Center for Integrative Genomics, Bâtiment Génopode, 1015-Lausanne, Switzerland.

2: current address: MRC Laboratory of Molecular Biology, Francis Crick Avenue, Cambridge Biomedical Campus, Cambridge CB2 0QH, UK

*: Corresponding author: Vincent.dion@unil.ch

Keywords: Epigenome editing, synthetic biology, chromatin, gene expression, histone deacetylases, expanded CAG/CTG repeats.

Abstract

Epigenome editing is an attractive way to manipulate gene expression. However, editing efficiencies depend on the DNA sequence context in a manner that remains poorly understood. Here we developed a novel system in which any protein can be recruited at will to a GFP reporter. We named it ParB/ANCHOR-mediated Inducible Targeting (PInT). Using PInT, we tested how CAG/CTG repeat size affects the ability of histone deacetylases to modulate gene expression. We found that repeat expansion reduces the effectiveness of silencing brought about by HDAC5 targeting. This repeat-length specificity was abolished when we inhibited HDAC3 activity. Our data guide the use of these histone deacetylases in manipulating chromatin. PInT can be adapted to study the effect of virtually any sequence on epigenome editing.

Introduction:

Chromatin structure impinges on every DNA-based transaction, from replication and DNA repair to transcription. Thus, it is not surprising that epigenome editing is being harnessed both to understand basic molecular mechanisms and to treat disease[1]. Epigenome editing is now most commonly carried out via the use of the domain of a chromatin modifier, or EpiEffector, fused to a catalytically dead Cas9 (dCas9). The fusion protein is targeted to a locus of choice by way of a customizable single guide RNA (sgRNA)[2-10]. Examples of dCas9-mediated epigenome editing include altering chromatin states by either targeting Krüppel-associated box (KRAB)[6] or the histone acetyltransferase domain of p300[2], thereby reducing or promoting enhancer function, respectively. Moreover, epigenome editing using Cas9-based approaches have been used to modify disease phenotypes in cells and *in vivo*[11,12].

It is currently not possible to predict whether targeting a specific locus with a particular dCas9-EpiEffector fusion will result in efficient chromatin modification and alteration of gene expression. Several reasons have been proposed to account for this, ranging from the sequence of the sgRNA and the distance of its target from the transcriptional start site[3-5], the chromatin structure already present at the target locus[13-19], and/or the exact EpiEffector used[2,4,10,17,19]. Indeed, the same EpiEffector targeted at different loci can have very different effects[10,17], highlighting that DNA context affects EpiEffectors in ways that are not understood.

Some DNA sequences can have profound effects on nucleosome positioning and chromatin structure[20]. A prime example of this is the expansion of CAG/CTG repeats, which causes 14 different neurological and neuromuscular diseases[21,22]. In healthy individuals, these sequences have less than 35 repeats at any one disease locus. However, they can expand and reach up to thousands of triplets. Once expanded, CAG/CTG repeats lead to changes in gene expression in their vicinity and to a heterochromatic-like state[23-26]. How these repetitive sequences might affect epigenome editing is unknown.

Here, we developed a method to understand how DNA sequence context can influence epigenome editing efficiency. We named the system ParB/ANCHOR-mediated induced targeting

(PInT). With PInT, any protein of interest can be targeted near a sequence of choice. ParB, a bacterial protein, forms oligomers once it nucleates at its non-repetitive binding site, INT[27]. Fusing a protein of interest to ParB leads to the recruitment of many of the desired molecules to the INT locus. The targeting is inducible as we coupled ParB/ANCHOR to a chemically induced proximity (CIP) system derived from plants[28]. The target sequence is embedded in a GFP mini gene[29] such that the effect of targeting on gene expression is easily monitored. Using PInT, we uncovered an unexpected effect of expanded CAG/CTG repeats on the effectiveness of histone deacetylase 5 (HDAC5) to modulate gene expression and found that this was due to the catalytic activity of HDAC3.

Results:

ParB/ANCHOR-mediated induced targeting (PInT)

We designed PInT (Fig. 1) to be modular and highly controllable. It contains a GFP mini gene that harbours two GFP exons flanking the intron of the mouse *Pem1* gene[29,30]. A doxycycline-inducible TetOn promoter drives the expression of the reporter. This cassette is always inserted at the same genomic location as a single copy integrant in T-Rex Flp-In HEK293 cells. Inside the intron, we inserted a 1029 bp non-repetitive sequence, INT, that contains four binding sites for dimers of the *Burkholderia cenocepacia* ParB protein. Once bound to INT, ParB oligomerizes in a sequence-independent manner, recruiting up to 200 ParB molecules[31]. This ParB/ANCHOR system was first used in live yeast cells to visualize double-strand break repair[27]. More recently, it has been used to monitor the mobility of a genomic locus upon activation of transcription[32] and to visualize viral replication[33] in live mammalian cells. We made the system inducible by fusing ParB to a plant protein called ABSCISIC ACID INSENSITIVE (ABI), which dimerizes with PYRABACTIN RESISTANCE1-LIKE (PYL) upon addition of abscisic acid (ABA) to the culture medium[28]. ABA is a plant hormone that is not toxic to human cells, making this CIP system especially convenient. Within 319bp of the INT sequence, there is a cloning site that can be used to insert any DNA motif. Thus, fusing any protein of interest to PYL allows for full temporal control over the recruitment of a protein of interest near a DNA sequence of choice.

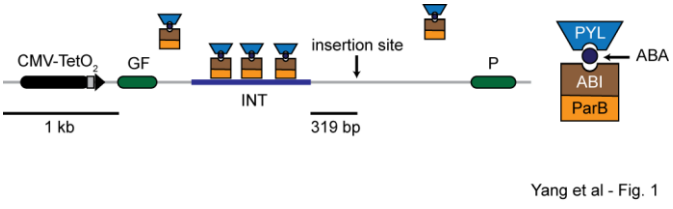

***Fig. 1:* Schematic of PInT**. *The GFP reporter is driven by an inducible Tet-On promoter. It contains an intron harbouring an INT sequence, which mediates the recruitment and oligomerization of ParB. We fused ParB to ABI, a plant protein that binds PYL only in the presence of abscisic acid (ABA). Fusing PYL to any protein of interest leads to its inducible recruitment 319bp away from a cloning site that can be used to insert a sequence of choice. The PYL construct contains a 3xFLAG tag whereas the ParB-ABI fusion includes 3xHA. They both contain SV40 nuclear localization signals.*

It was important to determine whether the components of PInT affect the expression of the GFP reporter. We first tested whether ABA changed GFP expression in GFP$(CAG)_0$ cells[29]. These cells carry the GFP mini gene without the INT sequence or any additional sequences in the intron (see

Table S1 and Fig. S1 for details on cell line construction). We found that treatment with up to at least 500 µM of ABA, which induces the dimerization between PYL and ABI, did not affect GFP expression (Fig. S2AB). We also transiently transfected GFP$(CAG)_0$ cells with plasmids expressing the ParB-ABI fusion. This had no detectable effect on the behaviour of the reporter (Fig. S2C). We next inserted the INT sequence inside the *Pem1* intron and integrated this construct using site-directed recombination, generating GFP-INT cells. These cells contain INT but no additional sequence within the intron. They do not express ParB-ABI. We found that the insertion of the INT sequence had little, if any, discernable effect on the GFP expression (Fig. S2D). We conclude that by themselves, the individual components of PInT do not significantly interfere with GFP expression.

We then stably integrated both the GFP-INT reporter and the ParB-ABI fusion to generate GFP-INT-B cells. We found a decrease in GFP expression that correlated with high levels of ParB-ABI (Fig. S2EFG), suggesting that the binding of ParB-ABI has a predictable effect on the GFP reporter. To avoid any complication, we integrated ParB-ABI early in the construction pipeline such that all the cell lines presented here contain the same amount of ParB-ABI (Fig. S1).

Next, we determined the efficiency of targeting PYL to the INT sequence and the consequences on GFP expression. We used nB-Y cells, which contain the GFP mini gene with the INT sequence, stably express both ParB-ABI (B) and PYL (Y), and contain n CAG repeats, in this case either 16, which is in the normal range, or an expanded repeat of 91 triplets (Fig. 2A, Fig. S3A). We found, using chromatin immunoprecipitation followed by qPCR (ChIP-qPCR), that only 0.1% of the input DNA could be precipitated when we treated the cells with the vehicle, DMSO, alone. By contrast, the addition of ABA to the cell media increased the association of PYL to the INT locus significantly, reaching 1.9 and 2.5% of the input chromatin pulled down in 16B-Y or 91B-Y cells, respectively (Fig. 2B). These results demonstrate the inducible nature of the system and show that the presence of the expansion does not interfere with the targeting efficiency. Importantly, PYL targeting had no effect on GFP expression as measured by flow cytometry (Fig. 2C). We conclude that PInT works as an inducible targeting system and that PYL targeting is efficient and does not further affect gene expression.

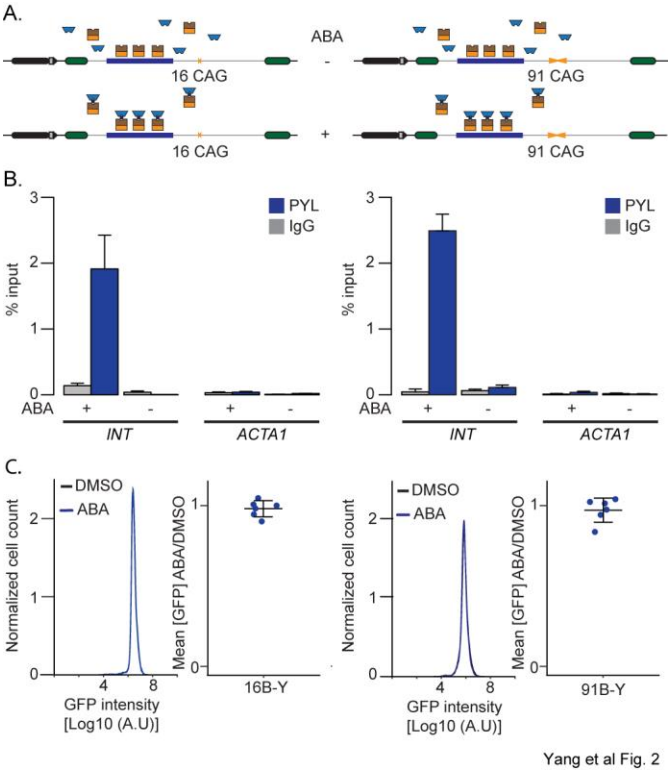

***Fig. 2:* Inducible targeting of PYL at the GFP reporter.** *A) Schematic representation of 16B-Y (left) and 91B-Y (right) cell lines. B) ChIP-qPCR using antibodies against FLAG to pull down PYL at INT and ACTA1 in 16B-Y cells (left, N=4) and 91B-Y cells (right, N=4). The error bars represent the standard error. C) Representative flow cytometry profiles as well as quantification of the GFP expression in 16B-Y (left, N=6) and 91B-Y (right, N=6) cells. The error bars are the standard deviation around the mean.*

HDAC5 silencing depends on CAG/CTG repeat size

We next sought to test whether we could manipulate GFP expression using HDAC5. This class IIa deacetylase impacts gene silencing and heterochromatin maintenance[34,35] as well as cell proliferation[35,36]. The PYL-HDAC5 fusion was functional since GFP-INT cells transiently expressing this fusion had slightly lower GFP expression than those expressing PYL alone (Fig. S4A). We created isogenic nB-Y-HDAC5 cells that express stably a PYL-HDAC5 fusion and have 16 or 59 CAG repeats within the GFP reporter (Fig. 3A). We found that adding ABA to these cells led to an increase in pull-down efficiency of PYL-HDAC5 at the INT locus from 0.06% to 2.2% in 16B-Y-HDAC5 cells and from 0.1% to 3% of input in the presence of 59 repeats (Fig. 3B). This was accompanied by a significant 2-fold decrease in GFP expression in 59B-Y-HDAC5 cells, whereas the decrease was of 3 folds in 16B-Y-HDAC5 cells (Fig. 3C, P=0.001 and P= 0.0015 using a paired Student's t-test comparing conditions with ABA to those with DMSO only in 16B-Y-HDAC5 and 59B-Y-HDAC5 cells, respectively). Remarkably, the decrease in expression was significantly lower in the context of an expanded repeat (Fig. 3C, P=0.0001 comparing the decrease in expression upon ABA addition between the 16B-Y-HDAC5 and 59B-Y-HDAC5 using a Student's t-test). Targeting efficiency of PYL-HDAC5 does not account for the repeat size-dependent effect since it was slightly higher in 59B-Y-HDAC5 than in 16B-Y-HDAC5 cells (Fig. 3B). To determine whether the effect is due to targeting at the INT locus, we transiently

expressed PYL-HDAC5 in GFP$(CAG)_0$B cells, which have no INT in their GFP reporter but express ParB-ABI. Adding ABA to these cells did not affect GFP expression (Fig. S4BC), suggesting that the presence of the INT sequence is essential. Moreover, PYL-HDAC5 targeting reduced the levels of acetylated histone H3 (acH3) (P=0.0001 and P=0.024 comparing DMSO treated and ABA-treated 16B-Y-HDAC5 and 59B-Y-HDAC5, respectively, using a Student's t-test), as measured by ChIP-qPCR. The decrease in acH3 upon targeting was greater in 16B-Y-HDAC5 than in 16B-Y cells (P=0.006 using a Student's t-test), consistent with a role for HDAC5 in silencing gene expression. Interestingly, the acH3 levels at the INT sequence were similar between 16B-Y and 91B-Y and between 16B-Y-HDAC5 and 59B-Y-HDAC5 (Fig. 3DE, P=0.95, and P=0.25, respectively using a Student's t-test), suggesting that the acH3 levels are unaffected by the expansion. We conclude that PYL-HDAC5 targeting silences better the lines with the shorter repeats.

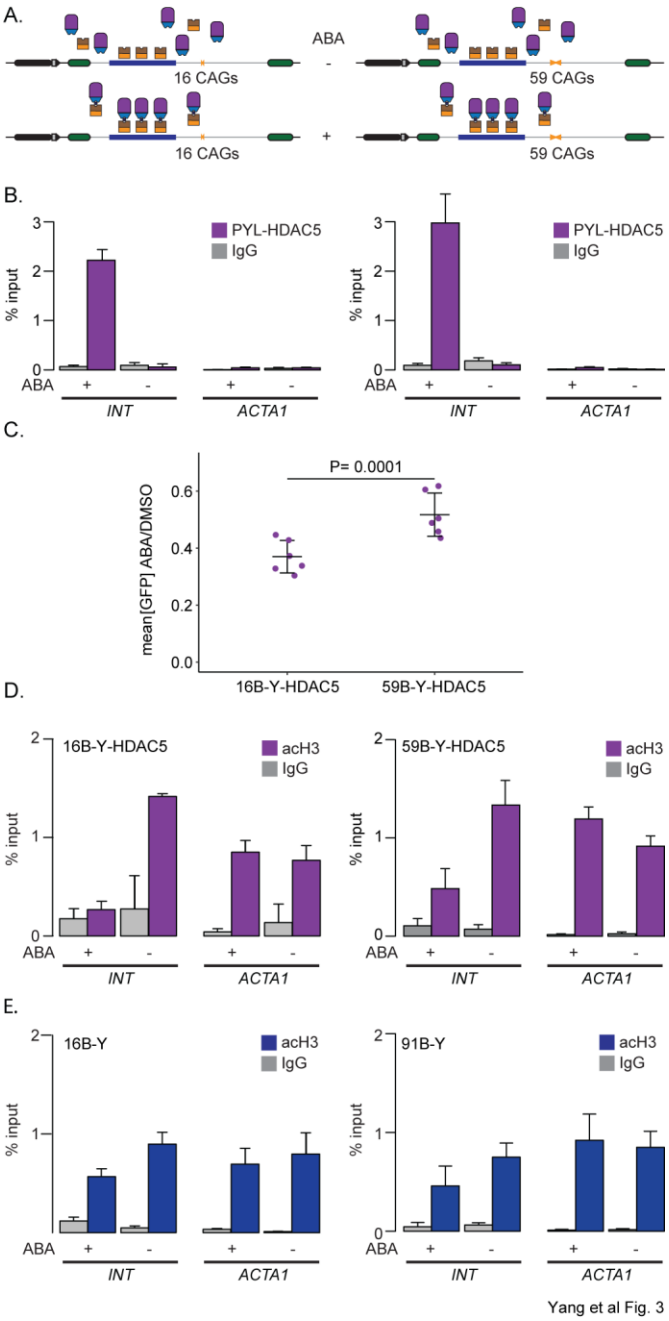

Fig. 3: ***PYL-HDAC5 targeting induces silencing in a repeat-length dependent manner****. A) Schematic representation of 16B-Y-HDAC5 (left) and 59B-Y-HDAC5 (right) cells. B) ChIP-qPCR using antibodies against FLAG to pull down PYL-HDAC5 at INT and ACTA1 in 16B-Y-HDAC5 cells (left, N=4) and 59B-Y-HDAC5 cells (right, N=4). The error bars represent the standard error. C) Quantification of GFP expression upon incubation with ABA or DMSO in 16B-Y-HDAC5 (left, N=6) and 59B-Y-HDAC5 (right, N=6) cells. The error bars show the standard deviation around the mean. D) ChIP-qPCR data using a pan-acetylated H3 antibody to pull down the INT and ACTA1 loci in 16B-Y-HDAC5 (left, N=4) and 59B-Y-HDAC5 (right, N=4) cells. The error bars represent the standard error. E) ChIP-qPCR data using a pan-acetylated H3 antibody to pull down the INT and ACTA1 loci in 16B-Y (left, N=4) and 91B-Y (right, N=4) cells. The error bars represent the standard error.*

The N-terminal domain of HDAC5 mediates silencing

Class I HDACs derive their catalytic activity *in vitro* from a conserved tyrosine residue that helps coordinate a zinc ion essential for catalysis[37]. By contrast, class IIa enzymes, like HDAC5, have a histidine instead of tyrosine at the analogous site, which considerably lowers HDAC activity[37]. In fact, the H1006Y mutant had more than 30-fold increase in its HDAC activity compared to the wild type enzyme[37]. To determine whether the catalytic activity of HDAC5 potentiates the decrease in GFP expression upon targeting, we compared the silencing activity of wild-type PYL-HDAC5, the H1006A loss-of-function mutant, and the H1006Y gain-of-function mutant by transient transfection in 40B cells, which contain the GFP-INT reporter with 40 CAGs and express ParB-ABI (Fig. 4A). The effect on silencing seen upon targeting of the wild-type PYL-HDAC5 fusion was lower when delivered by transient transfection compared to the stable cell lines. Nevertheless, under these conditions, targeting PYL-HDAC5-H1006A or PYL-HDAC5-H1006Y could both silence the transgene compared to targeting PYL alone (Fig 4B; P= 0.01 and 0.0008, respectively, using a Student's t-test), suggesting that tampering with the catalytic activity of HDAC5 does not influence silencing of our GFP reporter. Moreover, targeting PYL fused to the catalytic domain of HDAC5 did not shift GFP expression (Fig. 4B). Indeed, we find that the silencing activity was contained within the N-terminal part of HDAC5, which characterizes class IIa enzymes. Further truncations (Fig. 4AB) are consistent with a model by which the coiled-coil domain of HDAC5, which is responsible for homo and heterodimerization of class IIa enzymes *in vitro*[38], contains the silencing activity.

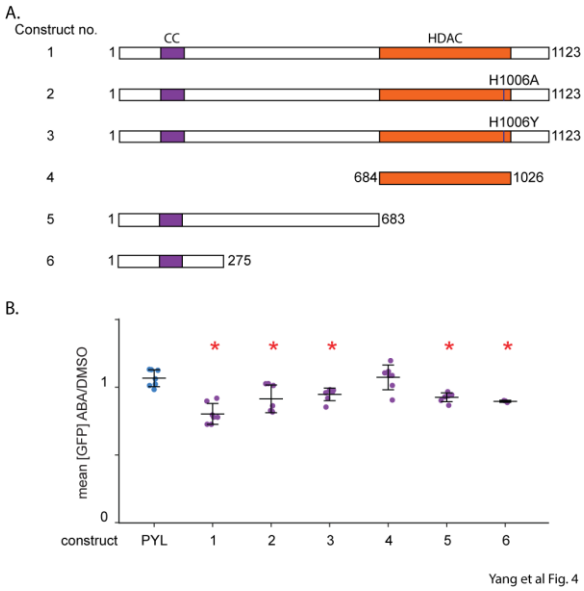

Fig. 4: The silencing activity of HDAC5 is contained in its N-terminal domain*. A) Mutants and truncations of HDAC5 fused to PYL. The coiled-coil (CC) domain is indicated in purple, the deacetylase domain (HDAC) in orange. B) Ratio of the mean GFP intensities in 40B cells between ABA and DMSO only treatment of 40B cells transiently transfected with plasmids containing the constructs shown in A. Construct 1: N=7, P=0.0002 versus PYL; construct 2: N=7, P=0.01 versus PYL; construct 3: N=7, P=0.0008 versus PYL; construct 4: N=7, P=0.88 versus PYL; construct 5: N=7, P=0.0012 versus PYL; construct 6: N=3, P=0.0003 versus PYL. In all cases,*

*we used a Student's t-test to calculate the P-values. The error bars show the standard deviation around the mean. *: P≤0.01 compared to PYL targeting.*

PYL-HDAC3 targeting enhances GFP expression independently of its catalytic activity

HDAC5 is thought to mediate histone deacetylation by recruiting other HDACs, including HDAC3[39]. Therefore, we hypothesized that PYL-HDAC3 targeting should have the same effect on GFP expression as PYL-HDAC5 targeting. To address this directly, we made a PYL-HDAC3 fusion and overexpressed it in 40B cells without targeting (Fig. S4D). We found that there was a slight decrease in GFP expression, suggesting that the construct could silence gene expression. Next, we generated nB-Y-HDAC3 cells and compared GFP intensities with and without ABA. Contrary to our initial hypothesis, we found that targeting PYL-HDAC3 in both 16B-Y-HDAC3 and 89B-Y-HDAC3 increased GFP expression by 1.5 fold (Fig. S5AB, P=0.0004 and P=0.001 using paired Student's t-tests comparing ABA and DMSO treatments in 16B-Y-HDAC3 and 89B-Y-HDAC3, respectively). The effect appeared direct since adding ABA to GFP$(CAG)_0$B cells transiently expressing PYL-HDAC3 did not affect GFP expression (Fig. S4E). The increase in GFP expression in nB-Y-HDAC3 cells was accompanied by an efficient targeting of the PYL-HDAC3 fusion (Fig. S5C) and an increase in acH3 levels (Fig. S5D). However, treatment with the HDAC3-specific small molecule inhibitor RGFP966[40] did not affect the increase in GFP expression in neither 16B-Y-HDAC3 nor 89B-Y-HDAC3 cells (Fig. S5E). We conclude that targeting PYL-HDAC3 increases GFP expression independently of its HDAC activity, consistent with the observation that HDAC3 has an essential role during development that does not involve its HDAC activity[41].

HDAC3 activity is required for the repeat size-specificity upon HDAC5-mediated silencing

Although HDAC3 targeting did not have the expected effect on GFP expression, evidence shows that its catalytic activity is implicated in HDAC5-mediated silencing[39]. To determine the potential catalytic role of HDAC3 in this context, we targeted PYL (Fig. 5A) or PYL-HDAC5 (Fig. 5B) to our GFP reporter in nB-Y and nB-Y-HDAC5 cells while cultivating the cells in the presence of RGFP966. We find that although this treatment had no effect on PYL targeting (Fig. 5A), it abolished the allele-length specificity of PYL-HDAC5 targeting, leading to a silencing efficiency of 2.4 and 2.5 folds for 16B-Y-HDAC5 and 59B-Y-HDAC5, respectively (Fig. 5B, P= 0.77 using a Student's t-test).

This is in contrast to the RGFP966-free conditions where targeting PYL-HDAC5 silenced better the normal-sized allele (Fig. 3). These results suggest that HDAC3 mediates the CAG repeat size-dependency upon PYL-HDAC5 targeting.

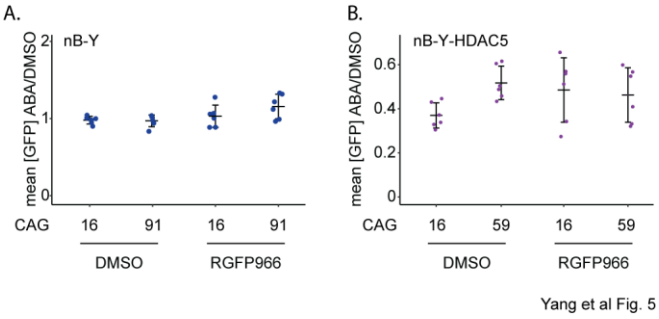

***Fig. 5:* HDAC3 activity is required for the allele-specificity upon HDAC5-mediated silencing**. *A) Quantification of GFP intensity upon targeting in the presence of RGFP966 or the vehicle, DMSO, in 16B-Y (N=6) and 91B-Y cells (N=6). Note that the data for the DMSO-treated cells is the same as in Fig. 2C. The addition of DMSO did not affect GFP expression, and we therefore pooled the data. B) Quantification of GFP intensity upon targeting in the presence of RGFP966 or the vehicle, DMSO, in 16B-Y-HDAC5 (N=6) and 59B-Y-HDAC5 cells (N=6). Note that the data for the DMSO-treated cells is the same as in Fig. 3C. The addition of DMSO did not affect GFP expression, and we therefore pooled the data. The error bars show the standard deviation around the mean.*

Discussion

We presented here a novel assay to investigate the effect of a DNA sequence of interest on the efficiency of a chosen EpiEffector in altering gene expression. As an example of how the DNA context may affect the activity of an EpiEffector, we showed that expanded CAG/CTG repeats decrease the silencing efficiency of HDAC5. Moreover, we determined that this allele-length specificity depends on HDAC3 activity, highlighting the potential of PInT in uncovering unique mechanistic insights. These data provide evidence that local DNA sequence context is an important determinant of epigenome editing, independently of the efficiency or mode of targeting.

PInT could be used for many different applications. First, the intron can host sequences beyond CAG/CTG repeats. Indeed, the GFP mini gene we used here, without the targeting components, was recently used to monitor the effect of a RNA polymerase III gene on RNA polymerase II-mediated transcription[42]. Second, it is often difficult to differentiate between a chromatin modifier changing gene expression because of a local effect on chromatin structure or indirectly through changes in the transcriptome. PInT allows making that distinction thanks to its inducible nature. Indeed, we found that overexpressing PYL-HDAC5 had a small effect on gene expression at the GFP reporter and that targeting it further decreased expression. We could conclude that PYL-HDAC5 can act locally to silence the transgene. This is useful in dissecting the mechanisms of action of EpiEffectors. Third, we demonstrated, using mutants and truncations of HDAC5, that we can quickly screen for protein domains and mutants that are most effective in modulating gene expression. Thus, PInT could be used to design peptides with sufficient activity to be useful in downstream epigenomic editing applications, for example when using dCas9 fusions *in vivo*. A current limitation of the *S. pyogenes* Cas9 for *in vivo* applications is its large size, which is at the limit of what adeno-associated viral vectors can accommodate[43]. Even with the smaller orthologues, fitting a dCas9 fusion inside a gene delivery vector is a challenge. Therefore, being able to trim an EpiEffector down to a small domain may help optimizing downstream applications and translation.

The observation that HDAC5 targeting has a differential effect on gene expression depending on the size of the repeat tract is surprising. Our data suggest that the deacetylase activity of HDAC3 is required for this effect. Importantly, we cannot currently rule out that RGFP966 may inhibit other HDACs that would be responsible for this effect. Nevertheless, this small molecule is highly selective for HDAC3[40], making this HDAC the most likely candidate for driving allele-specific silencing. HDAC3 could be setting up an asymmetry between the two size alleles in several ways. For instance, it could deacetylate histones (those residues not recognized by the pan-acetylated histone H3 antibody that we used) or non-histone proteins in the vicinity of the expanded CAG/CTG repeat prior to HDAC5 targeting. More work is required to understand further the mechanism of the repeat length-specific silencing.

Several studies have suggested that the ectopic insertion of an expanded CAG/CTG repeat in mice could induce changes in chromatin structure in the abutting sequences. An early example was the random insertion of arrays of transgenes, each carrying 192 CAGs[44], which led to the silencing of the transgenes independently of the site of genomic integration. In addition, inserting a 40 kb human genomic region containing the *DMPK* gene along with an expansion of 600 CTGs[45], or a 13.5Kb region containing the human SCA7 gene with 92 CAGS[46] all led to changes in chromatin marks near the expansion. It has been unclear, however, whether the presence of endogenous sequence elements, like CpG islands[47] and CTCF binding sites[26,48], is necessary for this effect. Our data show that 91 CAGs, without the flanking sequences normally present at the *DMPK* gene from whence this repeat was cloned[49], does not lead to significant changes in the levels of acetylated histone H3 in its vicinity. These data suggest that the flanking sequence elements play important roles in the induction and/or maintenance of heterochromatic marks surrounding expanded CAG/CTG repeats.

Recently, a number of studies have proposed that silencing the expanded repeat allele without affecting the expression of the normally sized allele may lead to a novel therapeutic approach for expanded CAG/CTG repeats[50-52]. However, only one factor, which is essential for mouse development[52], has been identified so far. We speculate that PInT may be adapted to screen for

allele length-specific silencers, which could help uncover novel therapeutic options for expanded CAG/CTG repeat disorders.

Materials and Methods

Cell culture conditions and cell line construction

The majority of the cell lines used, including all the parental lines, were genotyped by Microsynth, AG (Switzerland) and found to be HEK293.2sus. They were free of mycoplasma as assayed by the Mycoplasma check service of GATC Biotech. The cells were maintained in DMEM containing 10% FBS, penicillin, and streptomycin, as well as the appropriate selection markers at the following concentrations: 15 µg ml^{-1} blasticidin, 1µg ml^{-1} puromycin, 150µg ml^{-1} hygromycin, 400 µg ml^{-1} G418, and/or 400 µg ml^{-1} zeocin. The incubators were set at 37 °C with 5% CO_2. Whereas FBS was used to maintain the cells, dialyzed calf serum was used at the same concentration for all the experiments presented here. The ABA concentration used was 500 µM, unless otherwise indicated. Doxycycline (dox) was used at a concentration of 2 µg ml^{-1} in all experiments.

A schematic of cell line construction and pedigree is found in Figure S1, and the lines are listed in Table S1. This table includes the plasmids made for cell line construction. The plasmids used for transient transfections are found in Table S2. For each cell line, single clones were picked and tested for expression of ParB-ABI and PYL-fusions by western blotting using the protocol described before[30]. Briefly, whole cell extracts were obtained, and their protein content was quantified using the Pierce BCA Protein Assay Kit (ThermoScientific). Proteins were then run onto Tris-glycine 10% SDS PAGE gels before being transferred onto nitrocellulose membrane (Axonlab). The membranes were blocked using the Blocking Buffer for Fluorescent Western Blotting (Rockland), and primary antibodies were added overnight. Membranes were then washed followed by the addition of the secondary antibody (diluted 1 to 2000). The fluorescent signal was detected using an Odyssey Imaging System (Li-CoR). All antibodies used are found in Table S3. To assess repeat sizes, we amplified the repeat tracts using oVIN-0459 and oVIN-0460 with the UNG and dUTP-containing PCR as described[53] and then Sanger-sequenced by Microsynth AG (Switzerland). The sequences of all the primers used in this study are found in Table S4.

The ParB-INT sequence system used here is the c2 version described previsouly[27], except that the ParB protein was codon-optimized for expression in human cells. It is also called ANCHOR1 and is distributed by NeoVirTech. ParB-ABI (pBY-008), PYL (pAB-NEO-PYL), PYL-HDAC5 (pAB(EXPR-

PYL-HDAC5-NEO)) and PYL-HDAC3 (pAB(EXPR-PYL-HDAC3-NEO)) constructs were randomly inserted and single clones were then isolated (Table S1). GFP-reporter cassettes were inserted using Flp-mediated recombination according to the manufacturer's instruction (Thermo Scientific). Single colonies were picked and screened for zeocin sensitivity to ensure that the insertion site was correct.

Targeting assays

For targeting assays involving transient transfections, cells were plated onto poly-D-lysine-coated 12-well plates at a density of $6x10^5$ cells per well and transfected using 1 µg of DNA per well and Lipofectamine 2000 or Lipofectamine 3000 (Thermofisher Scientific). 6 hours after transfection, the medium was replaced with one containing dox and ABA or DMSO. 48h after the transfection, the cells were split, and fresh medium with dox and ABA or DMSO was replenished. On the fifth day, samples were detached from the plate with PBS + 1 mM EDTA for flow cytometry analysis.

In the case of the stable cell lines, cells were seeded at a density of $4x10^5$ per well in 12-well plates. The media included dox and ABA or DMSO. The medium was changed 48 hours later and left to grow for another 48 hours. The cells were then resuspended in 500µl PBS + 1 mM EDTA for flow cytometry analysis.

Flow cytometry and analysis

We used an Accuri C6 flow cytometer from BD and measured the fluorescence in at least 12 500 cells for each treatment. The raw data was exported as FCS files and analyzed using FlowJo version 10.0.8r1.

Chromatin immunoprecipitation

For chromatin immunoprecipitation, the cells were treated as for the targeting experiments except that we used 10 cm dishes and $4x10^6$ cells. After 96 hours of incubation, paraformaldehyde was added to the medium to a final concentration of 1% and the cells were incubated for 10 minutes at room temperature. The samples were then quenched with 0.125 M PBS-glycine for 5 minutes at room temperature. Samples were then centrifuged, the supernatant was discarded, and the cell pellets were washed with ice-cold PBS twice. The samples were split

into 10^7 cell aliquots and either used immediately or stored -75 °C for later use. Sonication was done using a Bioruptor for 25 to 30 min. DNA shearing was visualized by agarose gel electrophoresis after crosslink reversal and RNase treatment. 20% of sonicated supernatant was used per IP, with 3 µg anti-FLAG (M2, Sigma), anti-PAN acetylated H3 (Merck), or anti-IgG (3E8, Santa Cruz Biotechnology) on Protein G Sepharose 4 Fast Flow beads (GE healthcare). The samples were incubated at 4°C overnight and then washed with progressively more stringent conditions. After the IP, the samples were de-crosslinked and purified using a QIAquick PCR purification kit (Qiagen) and analyzed using a qPCR.

Quantitative PCR

Quantitative PCR was performed with the FastStart Universal SYBR Green Master Mix (Roche) using a 7900HT Fast Real-Time PCR System in a 384-Well Block Module (Applied Biosystems™). Primers used to detect enrichment at the INT sequence and at *ACTA1* gene are listed in Table S4. Ct values were analyzed using the SDS Software v2.4. The percentage of input reported was obtained by dividing the amount of precipitated DNA for the locus of interest by the amount in the input samples multiplied by 100%.

Statistics

We determined statistical significance in the targeting experiments using a two-tailed paired Student's t-test because the samples treated with DMSO and ABA were from the same original population and treated side-by-side. For the ChIP samples, the test used was a two-tailed Student's t-test. All the statistical analyses were done using R studio version 3.4.0. We concluded that there was a significant difference when $P < 0.05$.

Acknowledgements

We thank John H. Wilson and Kerstin Bystricky for sharing reagents as well as Fisun Hamaratoglu, Helder C. Ferreira, Ana C. Marques, Johanna E. Martin, and Nastassia Gobet for critical reading of the manuscript. This work was funded by SNSF professorship grants #144789 and #172936 to V.D.

Author contributions:

BY performed the experiments except for those presented in Fig. 4, which were done by ACB. ACB and LA helped BY in generating the cell lines. BY, ACB, and VD designed the experiments. BY and VD wrote the paper and prepared the figures.

References

1. Kungulovski, G. & Jeltsch, A. Epigenome Editing: State of the Art, Concepts, and Perspectives. *Trends Genet* **32**, 101-113 (2016).
2. Hilton, I.B. et al. Epigenome editing by a CRISPR-Cas9-based acetyltransferase activates genes from promoters and enhancers. *Nat Biotechnol* **33**, 510-7 (2015).
3. Gilbert, L.A. et al. Genome-Scale CRISPR-Mediated Control of Gene Repression and Activation. *Cell* **159**, 647-61 (2014).
4. Gilbert, L.A. et al. CRISPR-mediated modular RNA-guided regulation of transcription in eukaryotes. *Cell* **154**, 442-51 (2013).
5. Qi, L.S. et al. Repurposing CRISPR as an RNA-guided platform for sequence-specific control of gene expression. *Cell* **152**, 1173-83 (2013).
6. Thakore, P.I. et al. Highly specific epigenome editing by CRISPR-Cas9 repressors for silencing of distal regulatory elements. *Nat Methods* **12**, 1143-9 (2015).
7. Liu, X.S. et al. Editing DNA Methylation in the Mammalian Genome. *Cell* **167**, 233-247 e17 (2016).
8. Vojta, A. et al. Repurposing the CRISPR-Cas9 system for targeted DNA methylation. *Nucleic Acids Res* **44**, 5615-28 (2016).
9. Kearns, N.A. et al. Functional annotation of native enhancers with a Cas9-histone demethylase fusion. *Nat Methods* **12**, 401-403 (2015).
10. O'Geen, H. et al. dCas9-based epigenome editing suggests acquisition of histone methylation is not sufficient for target gene repression. *Nucleic Acids Res* **45**, 9901-9916 (2017).
11. Liao, H.K. et al. In Vivo Target Gene Activation via CRISPR/Cas9-Mediated Trans-epigenetic Modulation. *Cell* **171**, 1495-1507 e15 (2017).
12. Liu, X.S. et al. Rescue of Fragile X Syndrome Neurons by DNA Methylation Editing of the FMR1 Gene. *Cell* **172**, 979-992 e6 (2018).
13. Isaac, R.S. et al. Nucleosome breathing and remodeling constrain CRISPR-Cas9 function. *Elife* **5**(2016).
14. Horlbeck, M.A. et al. Nucleosomes impede Cas9 access to DNA in vivo and in vitro. *Elife* **5**(2016).
15. Jensen, K.T. et al. Chromatin accessibility and guide sequence secondary structure affect CRISPR-Cas9 gene editing efficiency. *FEBS Lett* **591**, 1892-1901 (2017).
16. Daer, R., Barrett, C.M. & Haynes, K.A. Histone modifications and active gene expression are associated with enhanced CRISPR activity in de-silenced chromatin. *BioRxiv* **10.1101/228601** (2018).
17. Kwon, D.Y., Zhao, Y.T., Lamonica, J.M. & Zhou, Z. Locus-specific histone deacetylation using a synthetic CRISPR-Cas9-based HDAC. *Nat Commun* **8**, 15315 (2017).
18. Lee, C.M., Davis, T.H. & Bao, G. Examination of CRISPR/Cas9 design tools and the effect of target site accessibility on Cas9 activity. *Exp Physiol* **103**, 456-460 (2018).
19. Cano-Rodriguez, D. et al. Writing of H3K4Me3 overcomes epigenetic silencing in a sustained but context-dependent manner. *Nat Commun* **7**, 12284 (2016).
20. Struhl, K. & Segal, E. Determinants of nucleosome positioning. *Nat Struct Mol Biol* **20**, 267-73 (2013).
21. Orr, H.T. & Zoghbi, H.Y. Trinucleotide repeat disorders. *Annu Rev Neurosci* **30**, 575-621 (2007).
22. Lopez Castel, A., Cleary, J.D. & Pearson, C.E. Repeat instability as the basis for human diseases and as a potential target for therapy. *Nat Rev Mol Cell Biol* **11**, 165-70 (2010).
23. Dion, V. & Wilson, J.H. Instability and chromatin structure of expanded trinucleotide repeats. *Trends Genet* **25**, 288-97 (2009).

24. Lopez Castel, A. et al. Expanded CTG repeat demarcates a boundary for abnormal CpG methylation in myotonic dystrophy patient tissues. *Hum Mol Genet* **20**, 1-15 (2011).
25. Barbe, L. et al. CpG Methylation, a Parent-of-Origin Effect for Maternal-Biased Transmission of Congenital Myotonic Dystrophy. *Am J Hum Genet* **100**, 488-505 (2017).
26. Cho, D.H. et al. Antisense transcription and heterochromatin at the DM1 CTG repeats are constrained by CTCF. *Mol Cell* **20**, 483-9 (2005).
27. Saad, H. et al. DNA dynamics during early double-strand break processing revealed by non-intrusive imaging of living cells. *PLoS Genet* **10**, e1004187 (2014).
28. Liang, F.S., Ho, W.Q. & Crabtree, G.R. Engineering the ABA plant stress pathway for regulation of induced proximity. *Sci Signal* **4**, rs2 (2011).
29. Santillan, B.A., Moye, C., Mittelman, D. & Wilson, J.H. GFP-based fluorescence assay for CAG repeat instability in cultured human cells. *PLoS One* **9**, e113952 (2014).
30. Cinesi, C., Aeschbach, L., Yang, B. & Dion, V. Contracting CAG/CTG repeats using the CRISPR-Cas9 nickase. *Nat Commun* **7**, 13272 (2016).
31. Khare, D., Ziegelin, G., Lanka, E. & Heinemann, U. Sequence-specific DNA binding determined by contacts outside the helix-turn-helix motif of the ParB homolog KorB. *Nat Struct Mol Biol* **11**, 656-63 (2004).
32. Germier, T. et al. Real-Time Imaging of a Single Gene Reveals Transcription-Initiated Local Confinement. *Biophys J* **113**, 1383-1394 (2017).
33. Mariame, B. et al. Real-time visualization and quantification of human Cytomegalovirus replication in living cells using the ANCHOR DNA labeling technology. *J Virol* (2018).
34. Lemercier, C. et al. mHDA1/HDAC5 histone deacetylase interacts with and represses MEF2A transcriptional activity. *J Biol Chem* **275**, 15594-9 (2000).
35. Peixoto, P. et al. HDAC5 is required for maintenance of pericentric heterochromatin, and controls cell-cycle progression and survival of human cancer cells. *Cell Death Differ* **19**, 1239-52 (2012).
36. Huang, Y., Tan, M., Gosink, M., Wang, K.K. & Sun, Y. Histone deacetylase 5 is not a p53 target gene, but its overexpression inhibits tumor cell growth and induces apoptosis. *Cancer Res* **62**, 2913-22 (2002).
37. Lahm, A. et al. Unraveling the hidden catalytic activity of vertebrate class IIa histone deacetylases. *Proc Natl Acad Sci U S A* **104**, 17335-40 (2007).
38. Backs, J., Backs, T., Bezprozvannaya, S., McKinsey, T.A. & Olson, E.N. Histone deacetylase 5 acquires calcium/calmodulin-dependent kinase II responsiveness by oligomerization with histone deacetylase 4. *Mol Cell Biol* **28**, 3437-45 (2008).
39. Fischle, W. et al. Enzymatic activity associated with class II HDACs is dependent on a multiprotein complex containing HDAC3 and SMRT/N-CoR. *Mol Cell* **9**, 45-57 (2002).
40. Malvaez, M. et al. HDAC3-selective inhibitor enhances extinction of cocaine-seeking behavior in a persistent manner. *Proc Natl Acad Sci U S A* **110**, 2647-52 (2013).
41. You, S.H. et al. Nuclear receptor co-repressors are required for the histone-deacetylase activity of HDAC3 in vivo. *Nat Struct Mol Biol* **20**, 182-7 (2013).
42. Yeganeh, M., Praz, V., Cousin, P. & Hernandez, N. Transcriptional interference by RNA polymerase III affects expression of the Polr3e gene. *Genes Dev* **31**, 413-421 (2017).
43. Epstein, B.E. & Schaffer, D.V. Combining Engineered Nucleases with Adeno-associated Viral Vectors for Therapeutic Gene Editing. *Adv Exp Med Biol* **1016**, 29-42 (2017).
44. Saveliev, A., Everett, C., Sharpe, T., Webster, Z. & Festenstein, R. DNA triplet repeats mediate heterochromatin-protein-1-sensitive variegated gene silencing. *Nature* **422**, 909-13 (2003).
45. Brouwer, J.R., Huguet, A., Nicole, A., Munnich, A. & Gourdon, G. Transcriptionally Repressive Chromatin Remodelling and CpG Methylation in the Presence of Expanded CTG-Repeats at the DM1 Locus. *J Nucleic Acids* **2013**, 567435 (2013).

46. Libby, R.T. et al. CTCF cis-regulates trinucleotide repeat instability in an epigenetic manner: a novel basis for mutational hot spot determination. *PLoS Genet* **4**, e1000257 (2008).
47. Gourdon, G., Dessen, P., Lia, A.S., Junien, C. & Hofmann-Radvanyi, H. Intriguing association between disease associated unstable trinucleotide repeat and CpG island. *Ann Genet* **40**, 73-7 (1997).
48. Filippova, G.N. et al. CTCF-binding sites flank CTG/CAG repeats and form a methylation-sensitive insulator at the DM1 locus. *Nat Genet* **28**, 335-43 (2001).
49. Gorbunova, V. et al. Selectable system for monitoring the instability of CTG/CAG triplet repeats in mammalian cells. *Mol Cell Biol* **23**, 4485-93 (2003).
50. Liu, C.R. & Cheng, T.H. Allele-selective suppression of mutant genes in polyglutamine diseases. *J Neurogenet* **29**, 41-9 (2015).
51. Liu, C.R. et al. Spt4 is selectively required for transcription of extended trinucleotide repeats. *Cell* **148**, 690-701 (2012).
52. Cheng, H.M. et al. Effects on murine behavior and lifespan of selectively decreasing expression of mutant huntingtin allele by supt4h knockdown. *PLoS Genet* **11**, e1005043 (2015).
53. Aeschbach, L. & Dion, V. Minimizing carry-over PCR contamination in expanded CAG/CTG repeat instability applications. *Scientific Reports* **7**, 18026 (2017).

Supplementary Information

Uncovering the Interplay between Epigenome Editing Efficiency and Sequence Context Using a Novel Inducible Targeting System

Bin Yang[1], Alicia C. Borgeaud[1,2], Lorène Aeschbach[1], and Vincent Dion[1]*

1: University of Lausanne, Faculty of Biology and Medicine, Center for Integrative Genomics, Bâtiment Génopode, 1015-Lausanne, Switzerland.

2: current address: MRC Laboratory of Molecular Biology, Francis Crick Avenue, Cambridge Biomedical Campus, Cambridge CB2 0QH, UK

*: Corresponding author: vincent.dion@unil.ch

Table S1: Cell lines

Cell line name	Parent cell line	Transgenes	Plasmid used	Integration method	Resistance marker	Reference
T-REX Flp-in	HEK293	pFRT/*lac*Zeo	-	-	Blasticidin Zeocin	Thermo Fisher
		Tetracycline Repressor	pcDNA6/TR	-		
$GFP(CAG)_0$	T-REX Flp-in	$GFP(CAG)_0$	$pGFP(CAG)_0$	Flp-mediated integration	Blasticidin Hygromycin	[29]
$GFP(CAG)_0B$	$GFP(CAG)_0$	$GFP(CAG)_0$	$pGFP(CAG)_0$	Flp-mediated integration	Blasticidin Puromycin Hygromycin	This study
		ParB-ABI*	pBY-008	Random integration		
GFP-INT	T-REX Flp-in	GFP-INT-CAG_0	pVIN-221	Flp-mediated integration	Blasticidin Hygromycin	This study
GFP-INT-B	GFP-INT	GFP-INT-CAG_0	pVIN-221	Site specific insertion	Blasticidin Puromycin Hygromycin	This study
		ParB-ABI*	pBY-008	Random integration		
GFP-INT-40	T-REX Flp-in	GFP-INT-CAG_{40}	pVIN-117	Flp-mediated integration	Blasticidin Hygromycin	This study
40-B	GFP-INT-40	GFP-INT-CAG_{40}	pVIN-117	Site specific insertion	Blasticidin Puromycin Hygromycin	This study
		ParB-ABI*	pBY-008	Random integration		
HEKB	T-REX Flp-in	ParB-ABI*	pBY-008	Random integration	Blasticidin Zeocin Puromycin	This study
HEKB-Y	HEKB	ParB-ABI*	pBY-008	Random integration	Blasticidin Zeocin Puromycin Neomycin	This study
		PYL†	pAB-NEO-PYL			
16B-Y	HEKB-Y	ParB-ABI*	pBY-008	Random integration	Blasticidin Puromycin Neomycin Hygromycin	This study
		PYL†	pAB-NEO-PYL			
		GFP-INT-CAG_{16}	pBY-050	Flp-mediated integration		
91B-Y	HEKB-Y	ParB-ABI*	pBY-008	Random integration	Blasticidin Puromycin Neomycin Hygromycin	This study
		PYL†	pAB-NEO-PYL			
		GFP-INT-CAG_{89}	pBY-018	Flp-mediated integration		

*: Contains 3xHA tag and a NLS. †: Contains 3xFLAG and a NLS.

Table S1 (continued): Cell lines

Cell line name	Parent cell line	Transgenes	Plasmid used	Integration method	Resistance marker	Reference
HEKB-Y-HDAC3	HEKB	ParB-ABI*	pBY-008	Random integration	Blasticidin Zeocin Puromycin Neomycin	This study
		PYL-HDAC3†	pAB(EXPR-PYL-HDAC3-NEO)			
16B-Y-HDAC3	HEKB-Y-HDAC3	ParB-ABI*	pBY-008	Random integration	Blasticidin Puromycin Neomycin Hygromycin	This study
		PYL-HDAC3†	pAB(EXPR-PYL-HDAC3-NEO)			
		GFP-INT-CAG_{16}	pBY-050	Flp-mediated integration		
89B-Y-HDAC3	HEKB-Y-HDAC3	ParB-ABI*	pBY-008	Random integration	Blasticidin Puromycin Neomycin Hygromycin	This study
		PYL-HDAC3†	pAB(EXPR-PYL-HDAC3-NEO)			
		GFP-INT-CAG_{89}	pBY-018	Flp-mediated integration		
HEKB-Y-HDAC5	HEKB	ParB-ABI*	pBY-008	Random integration	Blasticidin Zeocin Puromycin Neomycin	This study
		PYL-HDAC5†	pAB(EXPR-PYL-HDAC5-NEO)			
16B-Y-HDAC5	HEKB-Y-HDAC5	ParB-ABI*	pBY-008	Random integration	Blasticidin Puromycin Neomycin Hygromycin	This study
		PYL-HDAC5†	pAB(EXPR-PYL-HDAC5-NEO)			
		GFP-INT-CAG_{16}	pBY-050	Flp-mediated integration		
59B-Y-HDAC5	HEKB-Y-HDAC5	ParB-ABI*	pBY-008	Random integration	Blasticidin Puromycin Neomycin Hygromycin	This study
		PYL-HDAC5†	pAB(EXPR-PYL-HDAC5-NEO)			
		GFP-INT-CAG_{59}	pBY-018	Flp-mediated integration		

*: Contains 3xHA tag and a NLS. †: Contains 3xFLAG and a NLS.

Table S2: Plasmids used for transient transfection experiments

Name	Description	Source
pBY-008	Expresses ParB-ABI with 3xHA and a SV40 NLS	This study
pBY-022	Expresses PYL fused to 3xFLAG and a SV40 NLS. Also serves as a destination vector for making fusions	This study
pBY-006	Expresses PYL-HDAC3 with 3xFLAG and a SV40 NLS	This study
pBY-017	Expresses PYL-HDAC5 with 3xFLAG and a SV40 NLS	This study
pAB-HDAC5(mut-H-A)	Expresses PYL-HDAC5 H1006A with 3xFLAG and a SV40 NLS	This study
pAB-HDAC5(mut-H-Y)	Expresses PYL-HDAC5 H1006Y with 3xFLAG and a SV40 NLS	This study
pAB(EXPR-HDAC5-trunc1)	Expresses PYL-HDAC5 aa 1-275 with 3xFLAG and a SV40 NLS	This study
pAB-EXPR(PYL-cat_dom_HDAC5)	Expresses the PYL-HDAC5 catalytic domain with 3xFLAG and a SV40 NLS	This study
pAB-EXPR(PYL-Nterm_dom_HDAC5)	Expresses the PYL-HDAC5 N terminal domain fused to 3xFLAG and a SV40 NLS	This study

Table S3: Antibodies

Epitope	Company	Catalog number	Dilution	Assay
FLAG	Sigma-Aldrich	F1804-5MG	3 µg per IP	ChIP
			1:1000	WB
IgG	Santa Cruz Biotechnology	sc-69786	3 µg per IP	ChIP
Pan-acetylation of H3	Merck	#06-599	3 µg per IP	ChIP
Histone H3	Abcam	ab1791	3 µg per IP	ChIP
Actin	Sigma-Aldrich	A2066-.2ML	1:2000	WB

Table S4: Primers for qPCR and to verify repeat size

Oligo	Sequence	Targeted locus	Reference
oVIN-0459	5’ AAGAGCTTCCCTTTACACAACG	GFP transgene	[30]
oVIN-0460	5’ TCTGCAAATTCAGTGATGC	GFP transgene	[30]
oVIN-0969	5’ TGAATACCATGCGCTCTA	INT	This study

oVIN-0970	5’ GCCGTTCGTGGCAGAGAT	INT	This study
oVIN-1075	5’ AGCGCGGCTACAGCTTCAC	*ACTA1*	This study
oVIN-1076	5’ CAGCCGTGGCCATCTCTT	*ACTA1*	This study

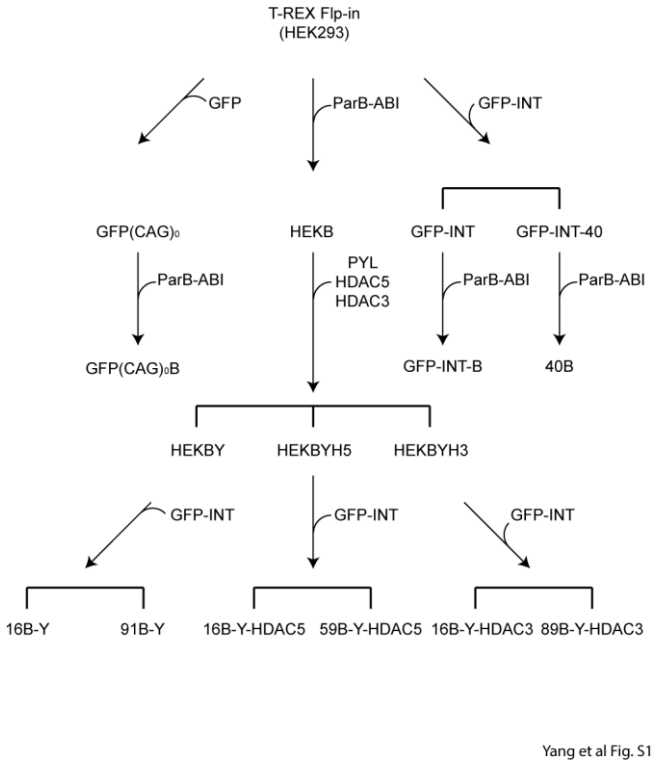

Fig. S1. Parentage of the cell lines described in this study. All cell lines are clonal.

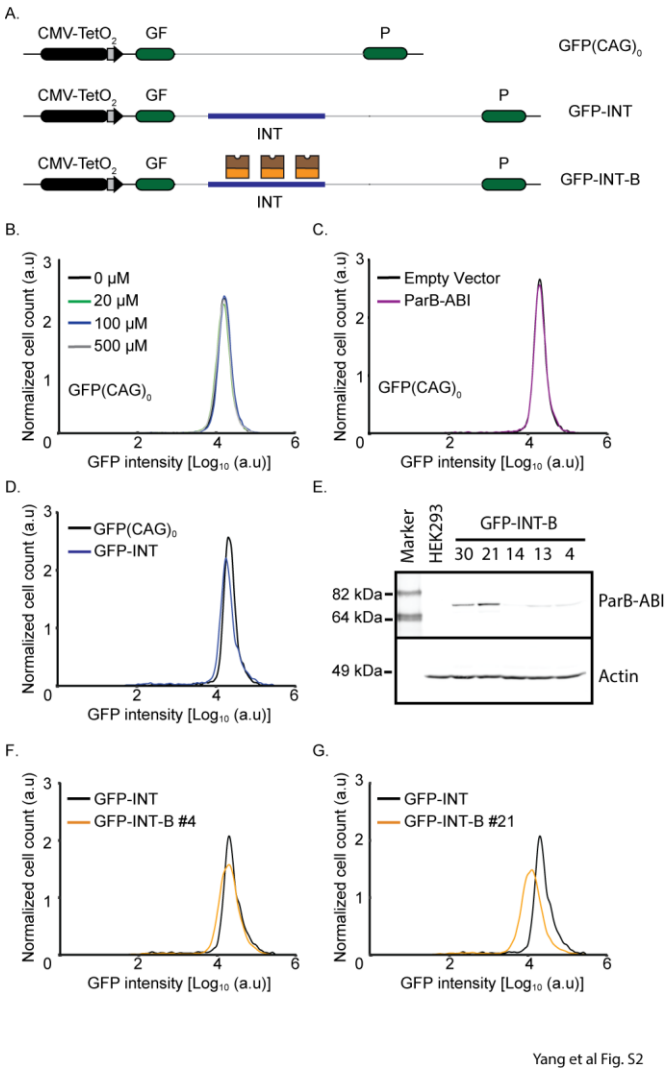

<u>Fig. S2.</u> Effect of components of PInT on GFP expression. A) Cartoon of cell lines used. B) Representative flow cytometry profiles of GFP(CAG)$_0$ cells treated with increasing concentrations of ABA dissolved into the same volume of DMSO. C) Representative flow cytometry profiles of GFP(CAG)$_0$ cell lines transfected with a plasmid expressing ParB-ABI or an empty vector. D) Comparison of GFP expression between GFP(CAG)$_0$ and GFP-INT cells. E) Western blots (against HA) of GFP-INT-B clones showing varying amounts of ParB-ABI in the different clones. F) Flow cytometry profiles of GFP-INT-B clone #4, which expresses low levels of ParB-ABI. G) Representative flow cytometry profile of GFP-INT-B clone #21 expressing a larger amount of ParB-ABI. Note that the GFP-INT parent profile is the same in panels F and G because the GFP expression of both clones was done on the same day using the same parent cell line control.

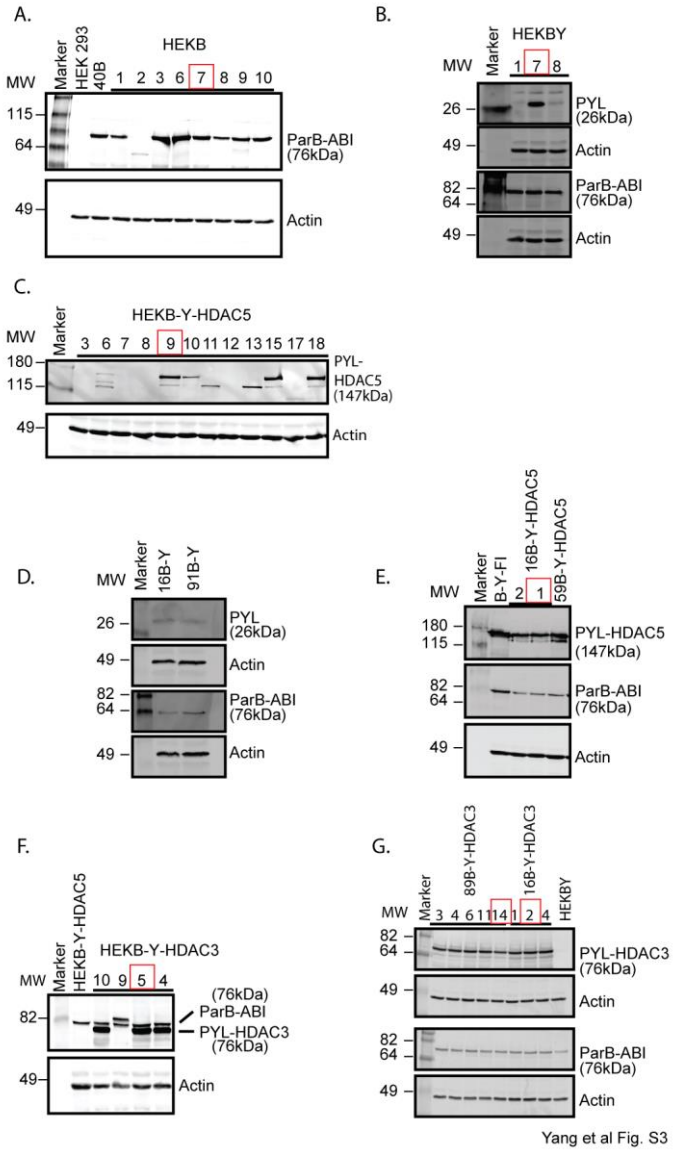

Fig. S3. Cell line making and characterization. The levels of ParB-ABI and PYL-fusions by western blotting using antibodies against HA and FLAG, respectively. The red boxes identify the clones that were used subsequently. A) ParB-ABI levels in HEKB clones. B) PYL levels in HEKBY cells. C) PYL-HDAC5 levels in HEKB-Y-HDAC5 cells. D) PYL-HDAC5 and ParB-ABI levels in 16B-Y-HDAC5 and 59B-Y-HDAC5 cells. nB-Y-FI cells will be characterized elsewhere. E) PYL-HDAC3 levels in HEKBYH3 cells. F) PYL-HDAC3 and ParB-ABI levels in 16B-Y-HDAC3 and 89B-Y-HDAC3 cells.

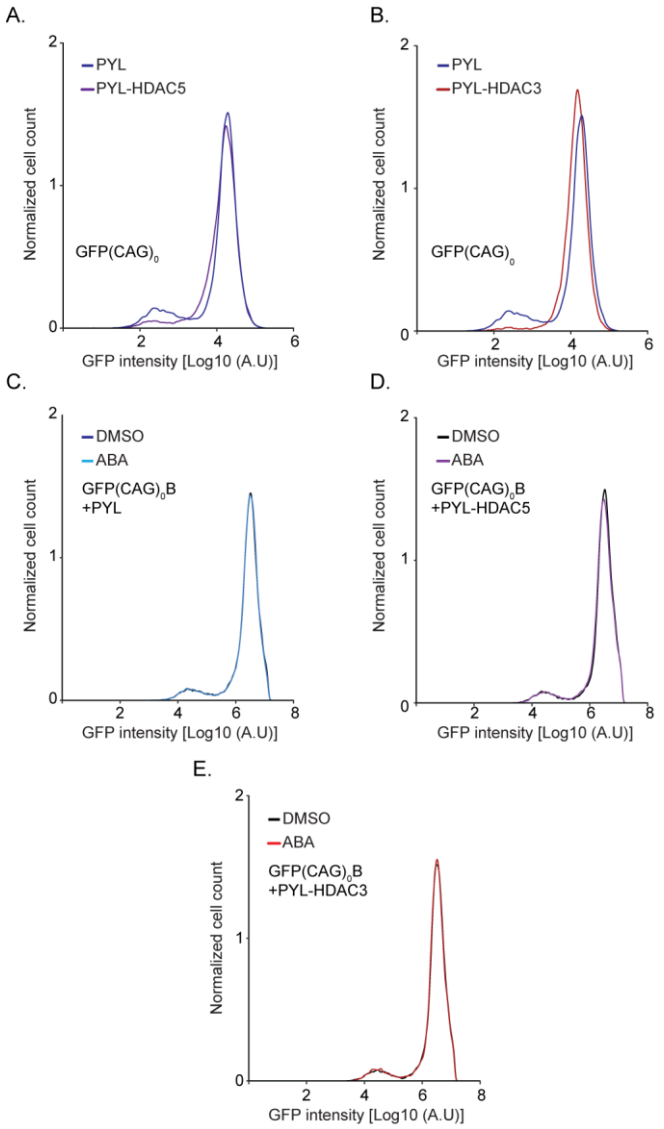

Yang et al Fig. S4

Fig. S4. The functionality of PYL fusions in GFP-INT-B cells and GFP(CAG)$_0$B cells. Representative flow cytometry profiles after transient overexpression of PYL and PYL-HDAC5 in GFP-INT-B cells (A), or of PYL and PYL-HDAC3 in GFP-INT-B cells (B). C-E) Representative flow cytometry profiles of GFP(CAG)$_0$B cells transiently transfected with PYL (C), PYL-HDAC5 (D), or PYL-HDAC3 (E) and incubated with DMSO or ABA.

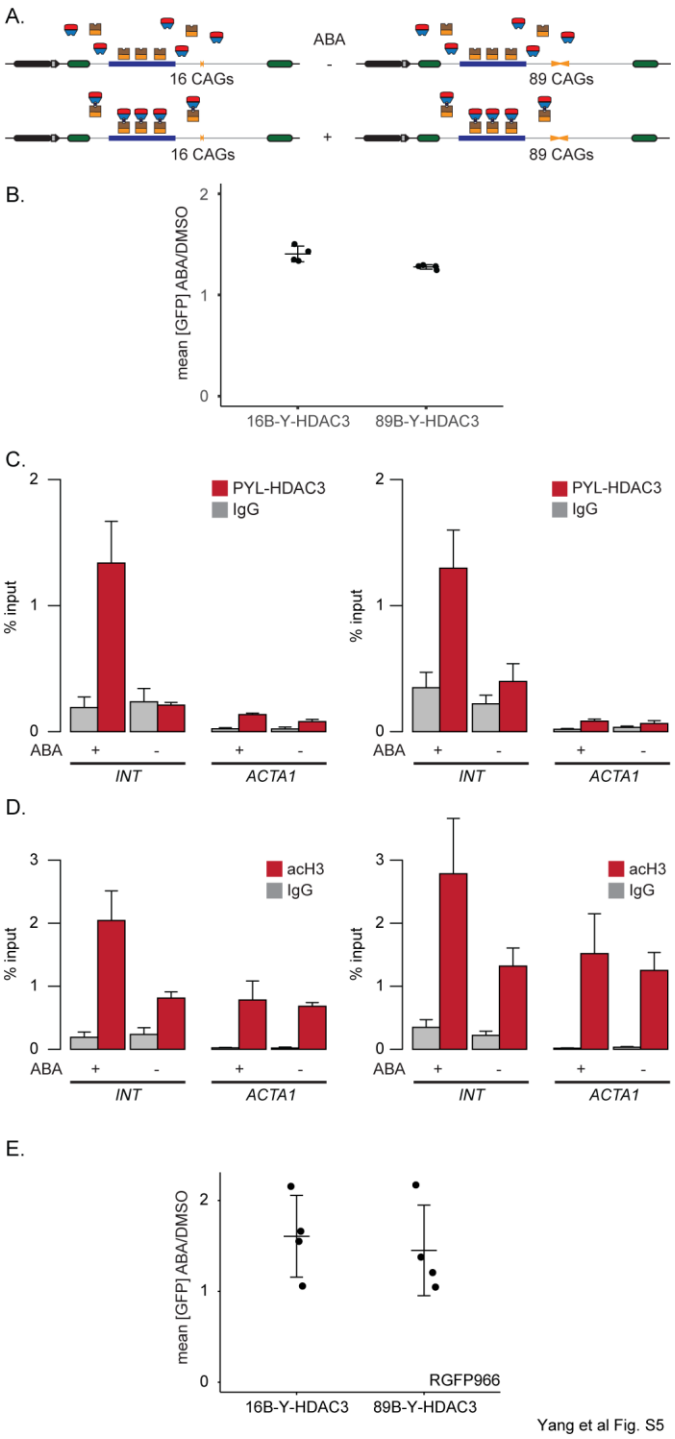

Fig. S5. Targeting of PYL-HDAC3 increases GFP expression independently of its catalytic activity. A) Schematic representation of the nB-Y-HDAC3 cells. B) Quantification of GFP expression in nB-Y-HDAC3 cells with ABA or DMSO (16B-Y-HDAC3: N=4; 89B-Y-HDAC3: N=4). The error bars are the standard error around the indicated mean. C) ChIP-qPCR experiments using an antibody against PYL-HDAC3 fusion (FLAG) at the INT and *ACTA1* loci in the presence of ABA or DMSO. Left, 16B-Y-HDAC3 cells (N=4), Right, 89B-Y-HDAC3 cells (N=4). The error bars are the standard error. D) ChIP-qPCR experiments using an antibody against pan-acetylated H3 (acH3) at the INT and *ACTA1* loci in the presence of ABA or DMSO. Left, 16B-Y-HDAC3 cells (N=4), Right, 89B-Y-HDAC3 cells (N=4). The error bars are the standard error. E) Quantification of GFP expression in nBYH3 cells with ABA or DMSO and treated with RGFP966 (16B-Y-HDAC3: N=4; 89B-Y-HDAC3: N=4). The error bars are the standard error around the indicated mean.

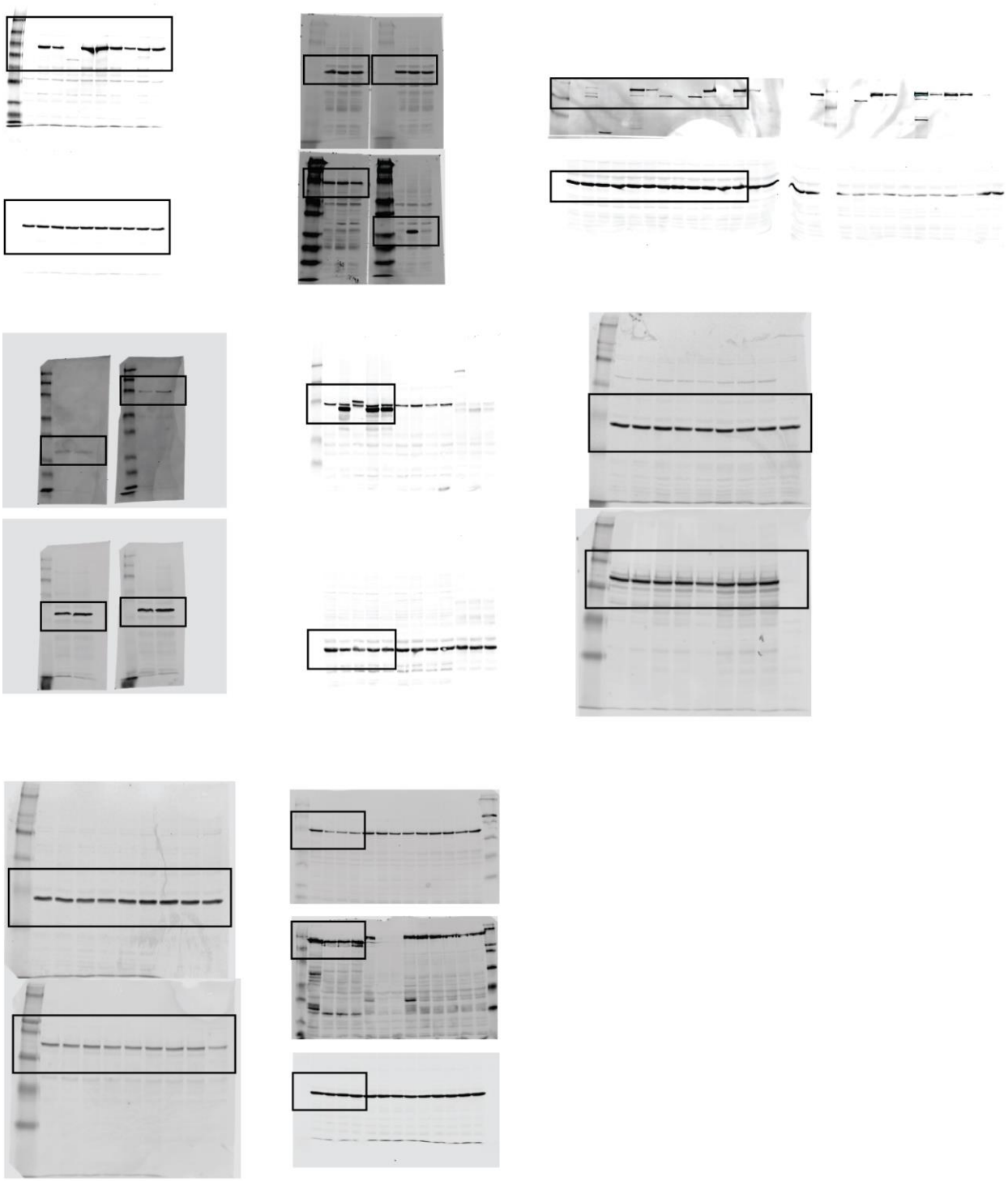

Yang et al Fig. S6

Fig. S6: Unaltered full western blots. Black boxes indicate where the blots were cropped.